

References and Notes

1. A. McEwen *et al.*, *Science* **288**, 1193 (2000).
2. R. Lopes-Gautier *et al.*, *Science* **288**, 1201 (2000).
3. A. McEwen *et al.*, *Icarus* **135**, 181 (1998).
4. The term "snowfield" in the context of Io means a flat plains area of certain spectral properties (1–3), and implied composition of S, SO₂ and/or silicate pyroclastic fragments or bedrock matrix. Significant SO₃ and some other S-compounds can be ruled out as major components based on the spectral data in the literature.
5. Terminology: Historical terms are pseudocraters, littoral cones, and rootless craters. Because we do not discuss the crater landforms, and because the word "littoral" has strong implications of seawater involvement, we later introduce the term "rootless conduit" for our specific discussion.
6. R. V. Fisher, *Geol. Rundsch.* **57**, 837 (1968).
7. _____ and H.-U. Schmincke, *Pyroclastic Rocks* (Springer-Verlag, Berlin, 1984), pp. 263–264.
8. M. M. Morrissey and T. Thordarson, *Eos* **72**, 566 (1991).
9. Z. Jurado-Chichay, S. Rowland, G. Walker, *Bull. Volcanol.* **57**, 471 (1996).
10. K. Wohletz and R. McQueen, in *Explosive Volcanism: Inception, Evolution, and Hazards*, Studies in Geophysics (National Academy Press, Washington, DC, 1984), chap. 12.
11. K. Wohletz, *Bull. Volcanol.* **48**, 245 (1986).
12. If the lava flows in the western delta were thinner than 1 m, they could not produce the extensive sheet flows observed in the I24 and I27 SSI images (1). If they were much thicker than 100 m, shadowed scarps would be visible at the flow margins. Based on the interpretation that the Prometheus lavas are inflated pahoehoe (1), and observations of similar inflated flows in the same size range on Earth, we suggest that the thickness of warm lava in the Prometheus lava "delta" is likely to be a few tens of meters.
13. We have based the density estimate on the assumption that the observed high temperatures for the lava flows (2) indicate a lava of mafic, that is, relatively dense, composition.
14. The triple point of S depends on a number of phase changes and ranges from 368 to 393 K. For lava at 1600 K, we assume $\rho = 2000 \text{ kg m}^{-3}$; $c = 1000 \text{ J kg}^{-1} \text{ K}^{-1}$; and $K = 3 \text{ W m}^{-1} \text{ K}^{-1}$. This gives $\kappa = 1.3 \times 10^{-6} \text{ m}^2 \text{ s}^{-1}$. For SO₂ ice or liquid at 130 K, we assume $\rho = 1600 \text{ kg m}^{-3}$; $c = 840 \text{ J kg}^{-1} \text{ K}^{-1}$; and $K = 3.5 \text{ W m}^{-1} \text{ K}^{-1}$ (a value obtained from low-temperature water-ice). This gives $\kappa \sim 2.6 \times 10^{-6} \text{ m}^2 \text{ s}^{-1}$. Latent heat released and absorbed can be ignored to the level of approximation here. Lava will release latent heat as it crystallizes; typical latent heats for magma crystallization are $\sim 500 \text{ kJ kg}^{-1}$. Under the fortuitous conditions considered here, the latent heat supplied by crystallization of the lava is almost exactly equal to the heat required for melting of the snow and the terms cancel in the conservation equations [M. Necati Ozisik, *Boundary Value Problems of Heat Conduction* (Dover, New York, 1968)]. Thermal conductivity could be appreciably lower if the lava is porous, or if temperatures are extremely high, perhaps by an order of magnitude. Lower values of thermal conductivity would extend the time scales calculated here.
15. B. A. Smith, E. M. Shoemaker, S. W. Kieffer, A. F. Cook II, *Nature* **280**, 738 (1979).
16. S. W. Kieffer, in *Satellites of Jupiter*, D. Morrison, Ed. (Univ. of Arizona Press, Tucson, AZ, 1982), fig. 18.5, p. 17.
17. H. S. Carslaw and J. C. Jaeger, *Conduction of Heat in Solids* (Clarendon, Oxford, ed. 2, 1959), p. 88.
18. L. Wilson and J. Head, *J. Geophys. Res.* **86**, 2971 (1981).
19. B. Kamb, *J. Geophys. Res.* **6**, 16585 (1991).
20. T. V. Johnson and L. A. Soderblom, in *Satellites of Jupiter*, D. Morrison, Ed. (Univ. of Arizona Press, Tucson, AZ, 1982), chap. 17, p. 637.
21. L. Wilson and J. W. Head, *Lunar Planet. Sci.* **XII**, 1191 (1981).
22. M. R. James and L. Wilson, *Lunar Planet. Sci.* **XXIX**, 1349 (1998) [CD-ROM].

23. Portions of this work were performed at the Jet Propulsion Laboratory, California Institute of Technology, under contract with NASA. We also thank T. Johnson for pointing out that we had Prometheus

bound if we had a mechanism to stop the motion of the plume.

28 February 2000; accepted 18 April 2000

Discovery of Gaseous S₂ in Io's Pele Plume

John R. Spencer,^{1*} Kandis Lea Jessup,² Melissa A. McGrath,³
Gilda E. Ballester,² Roger Yelle⁴

Spectroscopy of Io's Pele plume against Jupiter by the Hubble Space Telescope in October 1999 revealed absorption due to S₂ gas, with a column density of $1.0 \pm 0.2 \times 10^{16}$ per square centimeter, and probably also SO₂ gas with a column density of $7 \pm 3 \times 10^{16}$ per square centimeter. This SO₂/S₂ ratio (3 to 12) is expected from equilibration with silicate magmas near the quartz-fayalite-magnetite or wüstite-magnetite buffers. Condensed S₃ and S₄, probable coloring agents in Pele's red plume deposits, may form by polymerization of the S₂, which is unstable to ultraviolet photolysis. Diffuse red deposits near other Io volcanoes suggest that venting and polymerization of S₂ gas is a widespread feature of Io volcanism.

Io's plumes, discovered by Voyager in 1979, are the most dramatic expression of its active volcanism, and the 300-km-high Pele plume was by far the largest seen by Voyager (1). Galileo images have shown the Pele plume on only one occasion, in late 1996 (2). The plume was imaged by the Hubble Space Telescope (HST) at 257 to 291 nm, very faintly against dark sky in July 1995, and in extinction during transit of Io across Jupiter's disk in 1996 (3). In the transit images, the observed decrease in plume optical depth toward longer wavelengths was explained either by fine-grained dust scattering or SO₂ gas absorption; other gas species were not considered at that time. Subsequent transit and dark-sky imaging in July 1997 did not detect the plume, which was therefore less active then.

In October 1999 we observed the Pele plume with the HST (Table 1) to distinguish gas from dust extinction and to support observations by the Galileo spacecraft, which flew within 611 km of Io, and within 1300 km of the Pele plume vent, at 5:06 universal time (UT) (4) on 11 October. Images were taken with the Wide-Field Planetary Camera 2 (WFPC2) in the F255W, F336W, and F410M filters, with solar-weighted wavelength ranges of 257 to 291, 315 to 358, and 400 to 417 nm, respectively. Spectra were obtained during Jupiter transit with the Space Telescope Imaging Spectrograph (STIS), using its charge-coupled device (CCD) detector, its low-resolution 168- to 306-nm G230LB grat-

ing, and an effective slit size of 0.1×10 arc sec, giving 0.3-nm spectral resolution. The slit was stepped to five positions in 0.1-arc sec increments (relative to Io) perpendicular to its length, with an integration time of 255 s at each position and the expected location of the Pele vent placed within the central slit position.

The images taken against dark sky (Fig. 1) detected the Pele plume in the F255W and (probably) F336W filters, showing that the plume was active and had some dust component, because detectable Rayleigh scattering by gas alone is not expected at Io plume gas densities (5). The plume was conspicuous in the F255W image taken against Jupiter's disk, with an altitude of about 350 km, but was not seen in the F336W filter, confirming the wavelength dependence of the extinction (3). The plume was also invisible against Jupiter in 1.5-km/pixel resolution clear-filter (400 to 1000 nm) images taken on 11 October at 9:50 UT (4, 6).

The STIS data were processed as follows. Near-Io spectra are contaminated by the spectrum of Io's disk owing to the finite STIS pixel size and the HST point-spread function. To correct for this and establish the continuum level for the spectra, we combined the five STIS long-slit spectra into an image cube and fit Io's location in the image plane with a blurred model disk (7). We used the model to determine the fraction of the spectrum in each pixel (after blurring) that was contributed by Io's disk, and removed this contribution using an average Io spectrum taken from the regions of Io furthest from the limb. Grating-scattered light becomes significant at wavelengths below 240 nm and dominates the signal below 210 nm. We determined the scattered light level in the 210- to 220-nm region by comparing the depth of solar Fraunhofer lines in the data to those in a solar spectrum (8), and subtracted the scattered light

¹Lowell Observatory, 1400 West Mars Hill Road, Flagstaff, AZ 86001, USA. ²University of Michigan, Space Research Laboratory, 2455 Hayward Street, Ann Arbor, MI 48109, USA. ³Space Telescope Science Institute, 3700 San Martin Drive, Baltimore, MD 21218, USA. ⁴Department of Physics and Astronomy, Northern Arizona University, Flagstaff AZ 86011, USA.

*To whom correspondence should be addressed. E-mail: spencer@lowell.edu

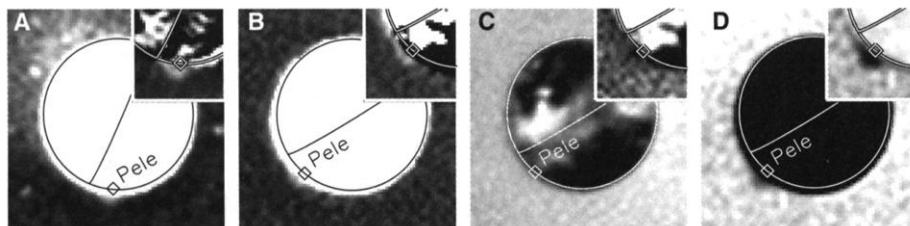


Fig. 1. October 1999 WPCF2 images of Io showing the Pele plume. (A) 10/09, 10:46 UT, F255W filter, plume faintly visible against the dark sky. (B) 10/11, 06:26 UT, F336W filter, plume probably visible against the dark sky. (C) 10/11, 06:44 UT, F336W filter, plume invisible against Jupiter. (D) 10/11, 06:47 UT, F225W filter, plume visible against Jupiter. Io's limb, equator, and the location of the Pele vent are shown. In the insets, plume visibility is enhanced by subtraction of a mean radial profile. Images have been sharpened by Lucy-Richardson deconvolution.

level thus determined on the assumption that scattered light contributed the same number of raw counts at all wavelengths. Scattered-light removal increased the depth of absorptions at short wavelengths. Spectra were then divided by an average Jupiter spectrum centered 0.35 arc sec from Pele. Although Jupiter's spectrum contains spatially variable NH_3 absorption in the 200- to 220-nm region (9), there was little spatial variation of the Jupiter spectra in the image cube over 0.35 arc sec, so our plume/Jupiter ratios are probably good approximations to the transmission spectrum of the plume.

Strong absorption lines due to the $\text{B}^3\Sigma_u^- \leftarrow \text{X}^3\Sigma_g^-$ band system of S_2 gas were conspicuous in several STIS spectra (Fig. 2). SO_2 absorption was also probably seen, with much lower signal-to-noise ratio (SNR) in the same spectra (Fig. 3). Ratios of images in the absorption bands to those in the intervening continuum reveal that the S_2 distribution is precisely centered above the Pele vent, and a similar concentration is seen, with low SNR, for SO_2 (Fig. 4).

We fitted the average of the three Pele spectra that showed the strongest S_2 absorption with isothermal models of S_2 and SO_2 gas absorp-

tion (10). Our best-fit spectrum (Fig. 2) gives an S_2 column density of $1.0 \pm 0.2 \times 10^{16} \text{ cm}^{-2}$ and rotational temperature of 300 K. SO_2 abundances are more uncertain because of the low SNR (Fig. 3) and systematic uncertainties due to the grating-scattered light removal; we estimate an SO_2 column density of $7 \pm 3 \times 10^{16} \text{ cm}^{-2}$ and a rotational temperature of 300 K (Fig. 3). Longward of 275 nm, S_2 and SO_2 both contribute to the spectrum; addition of SO_2 results in a lower best-fit temperature for the S_2 than for fits without SO_2 (Fig. 2). Both S_2 and SO_2 fits assume that the gas uniformly fills the three pixels that were averaged to create our "best" spectrum, and thus simplify what is undoubtedly a complex temperature and density distribution within the plume.

We believe that the SO_2 detection is probably real, despite the low SNR, for four reasons. (i) SO_2 models match the overall slope of the Pele spectrum shortward of 230 nm, and many of the individual absorption bands (Fig. 3). (ii) The S_2 and SO_2 band/continuum ratio images (Fig. 4) show significant correlation. Although noise produces spurious dark pixels in Fig. 4B, of the 150 spectra closest to Io, the three most S_2 -rich spectra (darkest pixels in Fig. 4A) are

among the eight darkest pixels in Fig. 4B. Monte Carlo simulations, which include an observed slightly higher noise level in the spectra closest to Io, show that such a correlation would occur by chance with a probability of only 4×10^{-4} . Also, the single darkest, most " SO_2 -rich," spectrum in Fig. 4B is one of the three most S_2 -rich spectra. (iii) Addition of SO_2 improves the shape of the spectrum between the S_2 lines longward of 275 nm (Fig. 2). The absolute level of the spectrum beyond 290 nm is underestimated by a few percent in the $\text{S}_2 + \text{SO}_2$ model, but this level is somewhat uncertain, depending on the accuracy of the correction for Io contamination. (iv) Similar local SO_2 concentrations have previously been inferred from spectroscopy of Io: 9×10^{16} to $2 \times 10^{18} \text{ cm}^{-2}$ above Loki [(11), reinterpreted by (12)]; 10^{17} to 10^{18} cm^{-2} (12); $\leq 2.1 \times 10^{17} \text{ cm}^{-2}$ (13); and $3.25 \times 10^{16} \text{ cm}^{-2}$ at Pele itself in 1996 (14).

S_2 has been detected in only two other astronomical contexts: the near-nucleus comae of comets (15, 16) and the impact sites of comet Shoemaker-Levy 9 (SL-9) on Jupiter (17). Its rarity is due in part to its short lifetime against ultraviolet (UV) photodissociation: 7.5 min at Earth's heliocentric distance (15), or 190 min at Jupiter. S_2 was seen at the SL-9 impact site 3 hours after impact, but was absent 22 days later (17). The 350-km height of the Pele plume implies, assuming ballistic trajectories, an ejection speed of 1.03 km s^{-1} and flight time of 24 min, much shorter than the photodissociation time scale.

The presence of S_2 gas in Io's plumes is not unexpected; sulfur vapor has been proposed as driver for the Pele plume (18), although the apparent dominance of SO_2 gas was not predicted. The relative abundance of the species S, S_2 , SO, and SO_2 can be used to infer temperatures and oxygen fugacities of the volcanic source region (19, 20). Our SO_2/S_2 ratio of 3 to 12

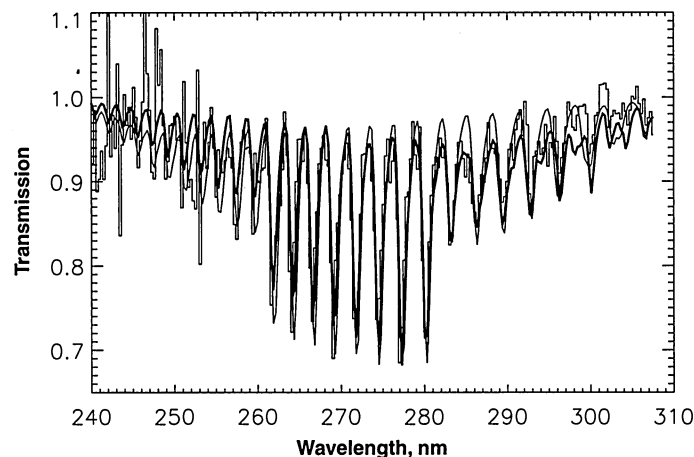
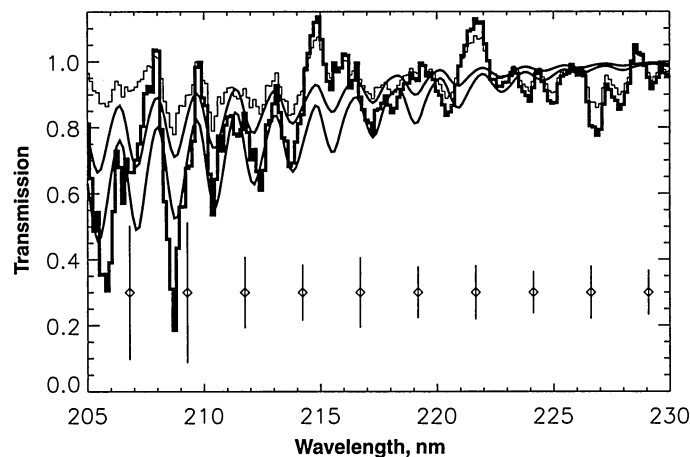


Fig. 2 (left). Spectrum of the Pele plume ratioed to Jupiter (stepped line), compared with our best-fit $\text{S}_2 + \text{SO}_2$ gas absorption model (heavy curve, see text) and our best-fit S_2 -only model (light curve) with column density $2 \times 10^{16} \text{ cm}^{-2}$ and temperature of 500 K. Spectra and models are binned to 0.28-nm resolution. **Fig. 3 (right).** Probable SO_2 absorption in the Pele plume before (light



stepped line) and after (heavy stepped line) correction for grating-scattered light. The smooth curves show models for SO_2 absorption with our estimated upper- and lower-abundance limits, 10×10^{16} and $4 \times 10^{16} \text{ cm}^{-2}$ of SO_2 at 300 K. Model and data are smoothed to 0.68-nm spectral resolution. Representative error bars show post-smoothing uncertainties due to photon statistics.

Table 1. Observation log.

Time range	Observation	Instrument and wavelength	Distance of Pele vent below limb
1999/10/09 10:46–11:28 UT	Imaging against dark sky	WFPC2, F255W, F336W, F410M	1–17 km
1999/10/09 12:33–12:56 UT	Spectroscopy against Jupiter	STIS, 180–310 nm	12–25 km
1999/10/11 06:13–06:39 UT	Imaging against dark sky	WFPC2, F255W, F336W, F410M	0–4 km
1999/10/11 06:44–06:54 UT	Imaging against Jupiter	WFPC2, F255W, F336W	5–9 km

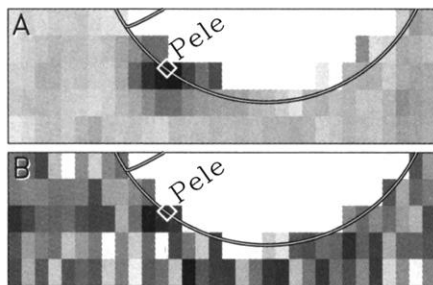


Fig. 4. Portion of the processed STIS image cube, showing the spatial distribution of S₂ (A) and SO₂ (B) absorption. The best-fit location of Io's limb, the equator, and the location of the Pele vent are shown. The images show the mean brightness in the individual S₂ or SO₂ absorption bands divided by the mean brightness at intervening continuum wavelengths; darker values imply stronger absorption. The white pixels on Io's disk were not considered; more pixels were excluded from the SO₂ image because of the lower SNR. Projected pixel size is 290 km by 145 km.

implies an oxygen fugacity near the quartz-fayalite-magnetite buffer if equilibrated with mafic magmas at 1400 K and 1- to 100-bar pressure, or near the wüstite-magnetite buffer if equilibrated with ultramafic magmas at 1800 K and similar pressures (19). Magma temperatures at Pele are known to reach at least 1370 K (21, 22). The relatively oxidized condition of the gas confirms the conclusion of Zolotov and Fegley (19) that Io's interior is free of metallic iron near the surface. The measured gas abundance, inferred 24-min flight time of the gas from the vent to the surface, and plume radius of 350 km give an equivalent resurfacing rate of 0.12 and 0.8 mm/year in the Pele plume deposits from S₂ and SO₂ gas, respectively (assuming a porous deposit with a density of 1 g cm⁻³), probably sufficient to explain albedo changes in the past 2.5 years seen by Galileo (23). The observations explain the discrepancy between previous imaging and spectroscopic estimates of SO₂ abundance at Pele: 10¹⁸ cm⁻² from imaging of Pele against Io's disk in 1993 (24) and 3.7 × 10¹⁷

cm⁻² from Jupiter transit imaging in 1996 (3), versus 3 × 10¹⁶ cm⁻² from spectroscopy 1 week after the transit images (14). The 260- to 280-nm extinction in the images was probably due to S₂, as in October 1999, rather than SO₂. The high transmission levels between the S₂ and SO₂ bands (Fig. 2) show that dust cannot have been a significant source of extinction in the October 1999 plume.

The discovery of S₂ also sheds light on the red color, perhaps due to S₃ and S₄ (25, 26), of the Pele plume deposits and other diffuse red deposits seen elsewhere on Io. If S₂ is broken down by UV photolysis shortly after deposition, production of red S₃ and S₄ molecules by polymerization may occur. The presence of smaller diffuse red deposits near many other active Io volcanoes (26) therefore suggests that S₂ gas is a common product of volcanic activity on Io. A question that remains is the fate of the SO₂ gas that (at least during the HST observations) appears to dominate over S₂ in the Pele plume. The 350-nm albedo of the Pele plume deposits is low, roughly 0.06, whereas SO₂ frost has an albedo of about 0.5 at this wavelength (27). However, near-infrared (NIR) spectra show that the plume deposits contain abundant SO₂ frost (28), consistent with the apparent SO₂-rich nature of the plume itself. A likely reconciliation of the reflectance data at the two wavelengths is that in the plume deposits the SO₂ is intimately mixed with the S₃ and S₄ (29). In the visible and near-UV the S₃ and S₄ are darker and dominate the spectrum, while the volumetrically dominant SO₂ is apparent in the NIR, where it has discrete absorption bands whereas the sulfur allotropes are bright and bland.

References and Notes

1. R. G. Strom, N. M. Schneider, R. J. Terrile, A. F. Cook, C. Hansen, *J. Geophys. Res.* **86**, 8593 (1981).
2. A. S. McEwen *et al.*, *Icarus* **135**, 181 (1998).
3. J. R. Spencer *et al.*, *Geophys. Res. Lett.* **24**, 2471 (1997).
4. Includes the 33 min of light-travel time from Jupiter to Earth.
5. S. A. Collins, *J. Geophys. Res.* **86**, 8621 (1981).

6. A. S. McEwen, personal communication.
7. A blank model disk of Io's known radius was convolved with a two-dimensional Gaussian function and fitted to the continuum image, with disk location, brightness, and Gaussian width as free parameters.
8. T. N. Woods *et al.*, *J. Geophys. Res.* **101**, 9541 (1996).
9. S. G. Edgington *et al.*, *Icarus* **142**, 342 (1999).
10. S₂ models were calculated at high spectral resolution by using energy-level constants for the ground electronic state (30), for the B state (31, 32), and spin-spin and spin-orbit constants (33). Honl-London factors are calculated for intermediate coupling between Hund's case a and b (34). Vibrational transition probabilities are from S. R. Langhoff and H. Partridge (personal communication). We assume a predissociation lifetime of 52 ps for transitions terminating on levels v' = 8, j' > 57, v' = 9, j' > 34, v' > 9. SO₂ modeling shortward of 2320 Å used the formulation of Ballester *et al.* (13) with improved modeling of temperature dependence based on new high-resolution measurements of SO₂ absorption cross section (35). At longer wavelengths, low-resolution SO₂ cross-section data (36) were used.
11. J. C. Pearl *et al.*, *Nature* **280**, 755 (1979).
12. E. Lellouch *et al.*, *Icarus* **98**, 271 (1992).
13. G. E. Ballester *et al.*, *Icarus* **111**, 2 (1994).
14. M. A. McGrath, M. J. S. Belton, J. R. Spencer, *Icarus*, in press.
15. M. F. A'Hearn, P. D. Feldman, D. G. Schleicher, *Astrophys. J.* **274**, L99 (1983).
16. M. F. A'Hearn *et al.*, *Bull. Am. Astron. Soc.* **31**, 1124 (1999).
17. K. S. Noll *et al.*, *Science* **267** 1307 (1997).
18. A. S. McEwen and L. A. Soderblom, *Icarus* **55**, 191 (1983).
19. M. Y. Zolotov and B. Fegley, *Icarus* **141**, 40 (1999).
20. _____, *Lunar Planet. Sci. XXXI*, abstract 2098 (2000) [CD-ROM].
21. A. S. McEwen *et al.*, *Science* **281**, 87 (1998).
22. A. G. Davies *et al.*, *Lunar Planet. Sci. XXX*, 1462 (1999) [CD-ROM].
23. A. S. McEwen *et al.*, paper presented at the American Geophysical Union fall meeting, San Francisco, 17 December 1999.
24. P. Sartoretti, M. J. S. Belton, M. A. McGrath, *Icarus* **122**, 273 (1996).
25. J. R. Spencer *et al.*, *Icarus* **127**, 221 (1997).
26. P. E. Geissler *et al.*, *Icarus* **140**, 265 (1999).
27. A. S. McEwen, *Icarus* **73**, 385 (1988).
28. S. Douté *et al.*, *Icarus*, in press.
29. A. S. McEwen, T. V. Johnson, D. L. Matson, L. A. Soderblom, *Icarus* **75**, 450 (1988).
30. A. L. Smith and J. B. Hopkins, *J. Chem. Phys.* **75**, 2080 (1981).
31. K. P. Huber and G. Herzberg, *Constants of Organic Molecules* (Van Nostrand Reinhold, New York, 1979).
32. V. E. Merchant and M. L. Andrews, *Appl. Opt.* **19**, 3113 (1980).
33. K. E. Meyer, D. R. Crosley, *Can. J. Phys.*, **51**, 2119 (1973).
34. J. B. Tatum and J. K. G. Watson, *Can. J. Phys.* **49**, 2693 (1971).
35. G. Stark *et al.*, *J. Geophys. Res.* **104**, 16585 (1999).
36. S. L. Mannatt and A. L. Lane, *J. Quant. Spectrosc. Radiat. Trans.* **50**, 267 (1993).
37. We thank A. Deet and C. Henry for help with data analysis, and A. McEwen, M. A'Hearn, D. Schleicher, I. Dashevsky, and J. Moses for valuable discussions. These observations were part of the HST/Galileo Io Campaign, and we thank campaign principal investigator F. Bagenal, N. Schneider, the rest of the campaign team, and the Space Telescope Science Institute for their invaluable help in bringing this work to fruition.

18 February 2000; accepted 17 April 2000